energies

MDPI

Article

A Study on the Modeling Method of Cage Slip and Its Effects on the Vibration Response of Rolling-Element Bearing

Ya Luo [1,2], Wenbing Tu [1,3], Chunyu Fan [4], Lu Zhang [4], Yudong Zhang [5] and Wennian Yu [4,*]

1 State Key Laboratory of Performance Monitoring and Protecting of Rail Transit Infrastructure, East China Jiaotong University, Nanchang 330013, China; luoya20022016@163.com (Y.L.); twb-2001@163.com (W.T.)
2 Rail Transit Technology Innovation Center, East China Jiaotong University, Nanchang 330013, China
3 School of Mechanotronics and Vehicle Engineering, East China Jiaotong University, Nanchang 330013, China
4 College of Mechanical and Vehicle Engineering, Chongqing University, Chongqing 400044, China; fanchunyu@cqu.edu.cn (C.F.); 202007131302@cqu.edu.cn (L.Z.)
5 School of Mechanical Engineering, Beijing Institute of Technology, Beijing 100081, China; zhang_yud@bit.edu.cn
* Correspondence: wennian.yu@cqu.edu.cn; Tel.: +86-136-7767-7243

Abstract: Rolling-element bearings play vital roles in the dynamic vibration performance of the whole machinery. Hence, accurate modeling and assessment of the rolling-element bearing are beneficial for the well understanding of the vibration response of rolling-element bearing. However, cage slip is usually ignored in the traditional rolling-element bearing modeling methods, which has a direct influence on the rotating speed and friction force of the rolling elements. To settle the modeling problem of rolling-element bearing with cage slip, in this study, a nonlinear dynamic model with multiple degrees of freedom of the roller bearing is established. The cage slip, the motion of each roller, nonlinear contact, damping, and friction are taken into consideration. With the proposed method, a nonlinear traction model is presented to describe the friction forces induced by cage slip. Furthermore, both the friction force acting on rolling elements and the effects of cage slip on the vibration response are investigated based on the established model. Some comparisons between the proposed modeling method with cage slip and the classical method without cage slip are made. The results show that the friction force applied to the balls increases with the cage slip, friction coefficient, rotational speed, and radial load. A slight cage slip could be beneficial for reducing the vibration energy of rolling-element bearing; however, it will result in more friction loss and impact components.

Keywords: rolling-element bearing; cage slip; friction force; dynamic modeling; vibration

Citation: Luo, Y.; Tu, W.; Fan, C.; Zhang, L.; Zhang, Y.; Yu, W. A Study on the Modeling Method of Cage Slip and Its Effects on the Vibration Response of Rolling-Element Bearing. *Energies* **2022**, *15*, 2396. https://doi.org/10.3390/en15072396

Academic Editors: Anil Kumar, Jing Liu, Jinglong Chen and Yimin Chen

Received: 9 February 2022
Accepted: 23 March 2022
Published: 24 March 2022

1. Introduction

Rolling-element bearings play vital roles in dynamic vibration performance, running stability, and service life of the whole machinery. It is of great significance to study the underlying dynamic characteristics of rolling-element bearing for mechanical maintenance, machine health monitoring, quality inspection, and design of rolling-element bearing [1]. Therefore, the accurate dynamic modeling of rolling-element bearings has attracted more and more attention in the field of the mechanical industry. It can provide theoretical guidance for the development of fault diagnosis techniques of rolling-element bearings [2,3].

Due to the special construction and functional principle of rolling-element bearing, even for a perfect bearing, the vibration is inevitable under the excitation sources such as varying compliance, radial clearance, and nonlinear contact relationship. The vibration caused by varying compliance is normally termed as varying compliance (VC) vibration. Many research works have been performed on the bearing VC vibration. For instance, Sunnersjö [4] presented a lumped parameter model that considers the two degrees of freedom (DOF) motion of the inner raceway based on the Hertzian contact theory to study

the VC vibrations of rolling-element bearing. Zhang et al. [5] investigated the resonant hysteresis of the VC vibrations for a rigid-rotor ball-bearing system using the harmonic balance method and Floquet theory. Yang et al. [6] and Jin et al. [7] conducted, respectively, an analytical study and an experimental study on the VC resonance of a rotor-bearing system. They found that the varying compliance contact resonance presents soft spring characteristics. Tomovic et al. [8] studied the effect of the number of rolling elements and radial clearance on the vibration of a rigid rotor when the rolling-element bearing is in the unloaded state. Xi et al. [9] presented a dynamic model for a spindle-bearing system to investigate the vibration response of the system under vairous cutting forces and rotating speeds.

Surface imperfections (e.g., waviness, roundness, off-size rolling elements, etc.) inevitably existed on the machined surfaces due to manufacturing errors, which are also additional excitation sources to the bearing vibration [10]. Kankar et al. [11] presented a dynamic analysis of a rigid rotor-bearing system with the consideration of the bearing surface waviness. Dipen and Patel [12] established a dynamic model to study the vibration responses of ball bearings with obvious raceway waviness. Liu et al. [13,14] introduced a displacement excitation model to study the coupling errors including the waviness and roundness of both raceways and balls. The effects of the order and amplitudes of the coupling errors on the vibrations of ball bearings were studied. Yu et al. [15] proposed an improved contact model between curved friction surfaces based on continuous length scales and fractal theory.

The bearing vibration responses generated by the defect on the raceway have been also widely studied, which are beneficial for bearing health monitoring. Singh et al. [16] established a dynamic finite element model of a rolling-element bearing that has a localized defect on the outer raceway. The generating mechanism of the dynamic contact loads between raceways and rolling elements and the relationship between external bearing vibration and the internal contact loads were explained. Li et al. [17] studied the dynamic responses of an angular contact ball bearing with the consideration of a defect on the outer raceway. The influences of some parameters on the internal contact load were investigated. Shah and Patel [18] developed a dynamic model to predict the vibration response of a ball bearing considering the masses of the shaft, raceways, ball, and housing. The vibrations of dry and lubricated contact bearings with local defects on the raceways were investigated. Liu et al. [19,20] proposed a revised time-varying displacement excitation model, and the effects of localized defects and offset are modeled. Qin et al. [21] established a nonlinear model for a high-speed ball bearing. The effects of time-dependent contact angles between balls and raceways were studied. The fault excitation was presented by a B-spline fitting curve.

Although there already exist a considerable number of studies on the vibration response of rolling-element bearing, most of them determined the cage speed according to pure-rolling assumptions, and the dynamic friction forces inside the bearing were neglected. However, when the rolling element is in contact with raceways, a combination of rolling and sliding motions occurs rather than a simple rolling motion [22]. Sawalhi and Randall [23] defined the angular position of the rolling element considering slippage, which was calculated based on the percentage variation in the mean impact frequency. Niu et al. [24] performed an intensive study on ball passing frequencies of rolling-element bearing, and the effects of three-dimensional motions and localize defects were included. Tu et al. [25,26] established a dynamic model to study the impacts between the cage and rolling elements when the bearing rotating speed fluctuates. Liu et al. [27] introduced a new model of a rolling-element bearing that can be used to study skidding characteristics. The novelty of this study is that the bearing cage is discretized so that its flexibility on the skidding can be modeled. Wang et al. [28] studied the skidding characteristics of angular contact ball bearing at high speed considering the dynamic contact between raceways and balls. It was found that the skidding behavior is significantly altered when an axial load is applied since the orbital and rotation speeds of balls are changed. Han and Chu [29]

established a three-dimensional model to study bearing skidding when both the radial and axial loads are applied to it. Han et al. [30] built another nonlinear dynamic model for skidding behavior with the influences of radial clearance and discontinuous contact considered. Selvaraj and Marappan [31] presented an experimental study to study the influences of some parameters (shaft speed, radial load, oil viscosity, number of rollers, etc.) on cage slip for various operating conditions. A non-dimensional parameter was introduced to predict the cage slip under any operating condition. To avoid breaking bearing structure while measuring the bearing cage slip, Zhan et al. [32] proposed a novel non-contact method to mesaure the cage slip using a magnetic field detection sensor. An adaptive de-noised method was used to increase the signal to noise ratio of the weak signal from the sensor.

From the above survey, it is concluded that most studies investigated the vibration responses of the rolling-element bearing via dynamic modeling with the consideration of numeral factors (e.g., varying compliance, surface imperfections, and localized defect) based on pure-rolling assumptions. There are some investigations considering the cage slip, which mainly concentrate on the effects of cage slip on the cage speed fluctuation, ball-cage impact frequency, and ball passing frequencies. There are a few experimental works focusing on measuring the cage slip under various operating conditions. As far as we know, variations in friction forces applied to the rolling element due to cage slip were not thoroughly studied. The dynamic responses of rolling-element bearings with various cage slip values have not been investigated. These constitute the major contribution of this study to the literature.

The purpose of this study is to investigate the effects of cage slip on the dynamic vibration response of rolling-element bearing. Therefore, a nonlinear dynamic model of rolling-element bearing is established considering the cage slip and the motions of rolling elements. This model includes nonlinear contact, damping, and friction forces. A nonlinear traction model is adopted to describe the friction forces induced by cage slip. The fourth-order Runge–Kutta method is used to solve the proposed model, and the bearing vibration response is simulated. The friction forces acting on the rolling element and the effects of cage slip on bearing vibration response are investigated.

2. Cage Slip Formulation and Friction Force Calculation

In the radial bearing applications of relatively low speed and sufficiently large load, non-sliding contacts between rolling elements and the raceways are assured. In these situations, the orbital speed of rolling elements, as well as the rotating speed of cage speed, is calculated by simple kinematics. For instance, when the outer raceway is fixed, the rotating speed of the cage is [33]

$$\omega_{ct} = \frac{1}{2}(1 - \frac{D}{d_m}cos\alpha)\omega_s \quad (1)$$

where ω_s is the rotating speed of the inner raceway; D denotes ball diameter; d_m is the bearing pitch diameter; α is the contact angle.

However, when the rolling-element bearing operates at a light load and a high speed, the centrifugal load of the rolling element aroused by the high speed increases to a level that cannot be neglected. The contact force between a rolling element and the inner raceway tends to decrease caused by the light load condition. Due to the centrifugal load, the radial clearance of rolling-element bearing increases, and the number of rolling elements contacting with the inner raceway reduces. The centrifugal load reaches the load between the rolling element and inner raceway under these situations. Therefore, the frictional drag forces at the outer raceway will exceed the frictional driving forces at the inner raceway, and the cage slip (also known as the skidding phenomenon) occurs. The cage speed will decrease to achieve a new equilibrium of drag and driving forces.

Cage slip is an important parameter to describe the skidding degree, which is given by

$$s_c = (1 - \omega_{ca}/\omega_{ct}) \times 100\% \tag{2}$$

where ω_{ca} denotes the actual value of cage speed. The larger the cage slip, the more severe the bearing skidding.

Therefore, the actual cage speed can be derived through Equation (2) as follows:

$$\omega_{ca} = (1 - s_c/100\%)\omega_{ct} \tag{3}$$

Once skidding occurs during bearing operation, the friction changes from rolling friction to sliding friction, as shown in Figure 1. When high sliding speeds develop due to cage slip, scuffing can be reached [34]. The sliding friction force is much larger and has an important effect on the vibration responses of the rolling-element bearing. It has a close relationship with the contact force and friction coefficient. To calculate the friction forces applied to the jth ball, sliding velocities at the contact surfaces of the inner and outer raceways are calculated first. The sliding velocities depend on the motions of bearing components. The velocities of contact points on each contact body can be determined according to the kinematical relationship as shown in Figure 2.

$$v_{ii,j} = \frac{1}{2}\omega_s d_m (1 - \frac{D}{d_m}\cos\alpha) \tag{4}$$

$$v_{ib,j} = \frac{1}{2}\omega_{ca} d_m (1 - \frac{D}{d_m}\cos\alpha) + \frac{1}{2}\omega_{b,j} D\cos\alpha \tag{5}$$

$$v_{ob,j} = \frac{1}{2}\omega_{ca} d_m (1 + \frac{D}{d_m}\cos\alpha) - \frac{1}{2}\omega_{b,j} D\cos\alpha \tag{6}$$

where $\omega_{b,j}$ is the rotational speed of the jth ball; $v_{ii,j}$ is the linear velocity of the inner raceway at the contact point with the jth ball; $v_{ib,j}$ and $v_{ob,j}$ are the linear velocities of the jth ball at the contact points with the inner raceway and outer raceway, respectively.

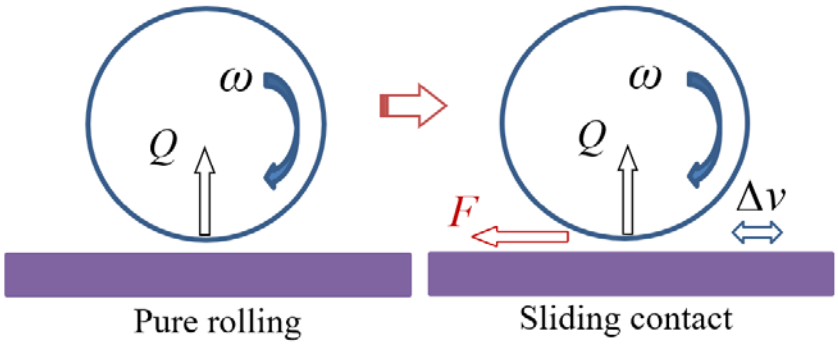

Figure 1. Sliding friction force due to skidding.

Thus, the sliding velocities at the contact surfaces of the inner and outer raceways are now given by

$$\Delta v_{i,j} = v_{ii,j} - v_{ib,j} = \frac{1}{2}(\omega_s - \omega_{ca}) d_m (1 - \frac{D}{d_m}\cos\alpha) - \frac{1}{2}\omega_{b,j} D\cos\alpha \tag{7}$$

$$\Delta v_{o,j} = v_{ob,j} = \frac{1}{2}\omega_{ca} d_m (1 + \frac{D}{d_m}\cos\alpha) - \frac{1}{2}\omega_{b,j} D\cos\alpha \tag{8}$$

The traction behavior of bearing lubricant is quite complex that involves the individual lubricant property, elastohydrodynamic (EHD) features, thermal effect, and the viscosity–pressure–temperature relationship in the high-pressure contact zone. Gupta presented an extensive summary on this subject in his book [35]. Bălan et al. [36] and

Olaru et al. [37] introduced a theoretical model and an experimental methodology to determine the traction torque in a modified thrust ball bearing. Since the motivation of this study was to investigate the influence of cage slip on the dynamic responses of rolling elements, a well-known simplified lubricant coefficient-slip relationship was adopted. Consideration of a sophisticated lubricant traction model could be one of our future research directions.

Figure 3 shows the simplified traction model in which the friction coefficient of the contact between rolling elements and raceways depends only on the sliding velocity. The friction coefficient increases linearly with the sliding velocity and remains unchanged (i.e., μ_m) beyond a certain value of sliding velocity (i.e., Δv_m). This traction model was used by many researchers to investigate the dynamic characteristics of rolling-element bearing [24,35,38,39]. It needs to be noted that the friction coefficient used in this model is independent of velocity, pressure, or temperature. However, as affirmed by Guta [35], this relationship between the friction and sliding velocity is justified for a solid lubricant, as considered in this study.

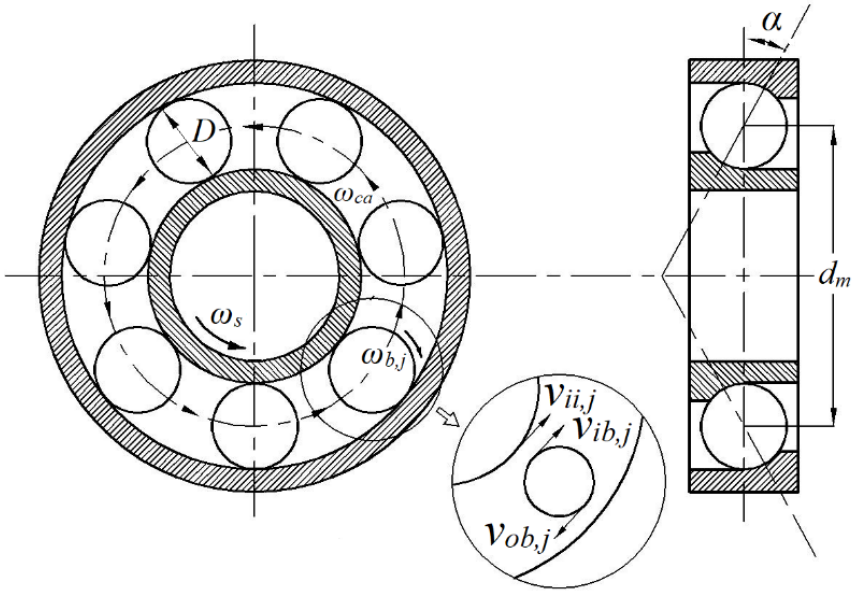

Figure 2. Kinematical relationship for a ball bearing.

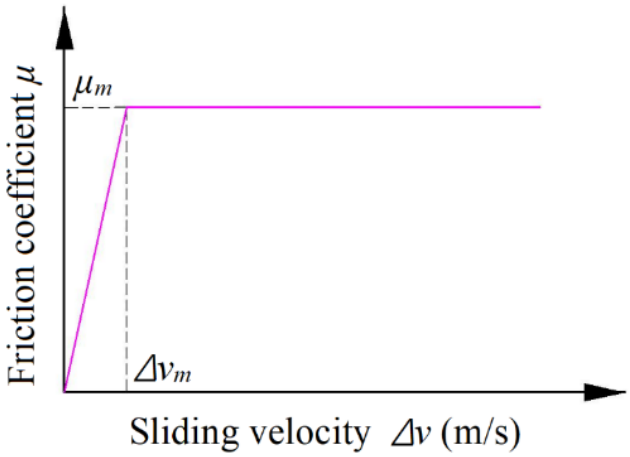

Figure 3. Relation between the friction coefficient and the sliding velocity.

The friction forces at the contact surfaces between rolling elements and raceways are

$$F_{in,j} = -\mu Q_{in,j} \frac{\Delta v_{i,j}}{|\Delta v_{i,j}|} \tag{9}$$

$$F_{out,j} = -\mu Q_{out,j} \frac{\Delta v_{o,j}}{|\Delta v_{o,j}|} \tag{10}$$

where $Q_{in,j}$ and $Q_{out,j}$ are the contact force between the jth ball and the inner raceway, and the contact force between the jth ball and the outer raceway, respectively.

3. Theoretical Formulation of the Dynamic Model

In this study, the ball bearing under investigation was modeled by a lumped parameter system. A dynamic model was built to study the influence of cage slip on bearing vibration, as shown in Figure 4. For a radially loaded ball bearing, some effective assumptions were made as follows:

1. Only plane motions of balls, cage, and raceways of the bearing were considered;
2. The balls were considered as mass points, and only the radial vibrations of the balls were taken into account;
3. The raceways were treated as rigid bodies, except the contact areas. Nonlinear contact deformations were considered at the contact zones between raceways and balls, which are consistent with the Hertz elastic contact theory;
4. The role of the cage was to maintain a constant spacing between the rolling elements; The cage was assumed to be rigid and maintained constant spacing between the balls. The cage speed was constant, and the interactions between the cage and balls were neglected;
5. The outer raceway was supported by a fixed housing, and the inner raceway was firmly fitted to the shaft.

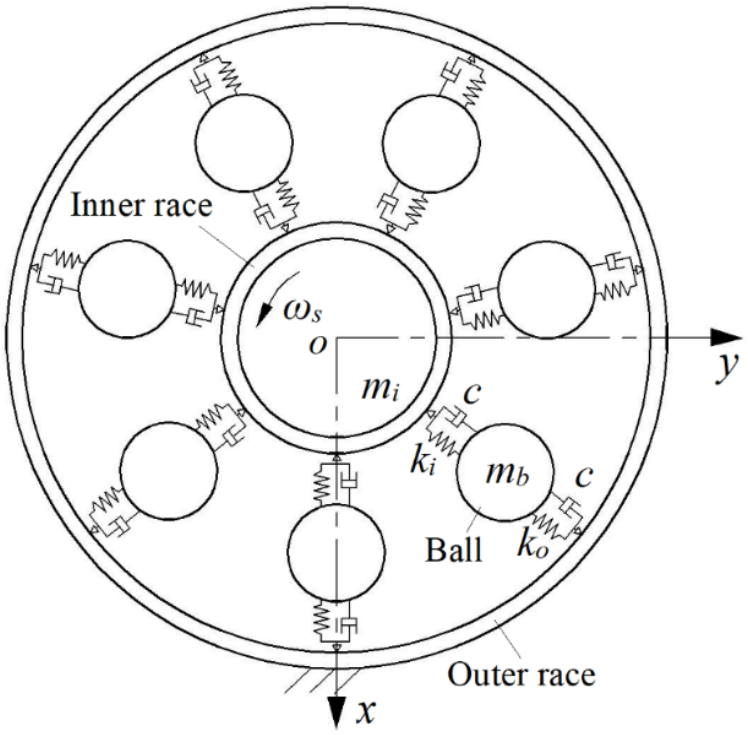

Figure 4. Diagram of the developed dynamic model of ball bearing.

3.1. Deformations and Contact Forces of Rolling Elements

To calculate the contact deformations between the jth ball and raceways, the radial displacement of the inner raceway at the jth ball position was first determined. Figure 5 shows the positions of the inner raceway before and after loading. The displacements of

the inner raceway along the x, y directions are x_s, y_s, respectively. The radial displacement of the inner raceway at the jth ball position is

$$d_{r,j} = x_s \cos\theta_j + y_s \sin\theta_j \tag{11}$$

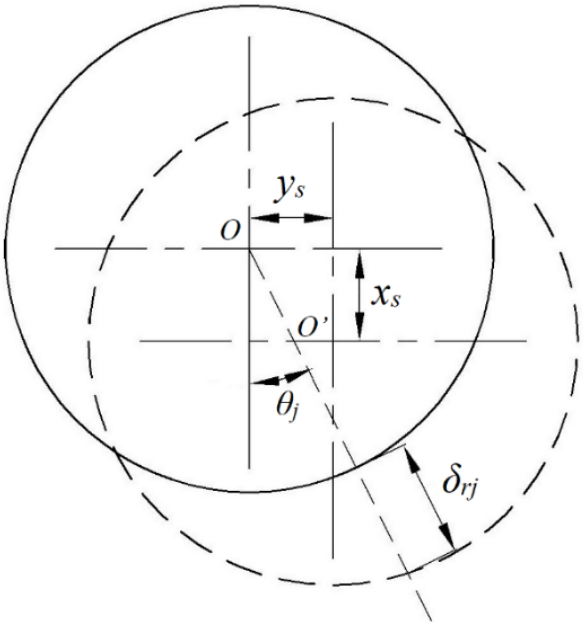

Figure 5. Radial displacement of the inner raceway at the jth ball position.

The angular position θ_j of the jth ball is defined as

$$\theta_j = (j-1)\frac{2\pi}{Z} + \omega_{ca}t \tag{12}$$

where Z indicates the number of balls.

The contact deformations between the jth ball and raceways depend on their relative motion and internal radial clearance of ball bearing. For the jth ball, the contact deformations are given as

$$\delta_{in,j} = \lambda_j(d_{r,j} - d_{br,j} - \frac{P_d}{2}) \tag{13}$$

$$\delta_{out,j} = \lambda_j(d_{br,j} - \frac{P_d}{2}) \tag{14}$$

where $d_{br,j}$ denotes the radial displacement of the jth ball; P_d refers to the radial clearance of ball bearing. Contact deformation is not allowed to be below zero at any time. Thus a contact coefficient λ_j is defined, which can be determined by

$$\lambda_j = \begin{cases} 1 & \delta_{in,j}, \delta_{out,j} > 0 \\ 0 & \delta_{in,j}, \delta_{out,j} \le 0 \end{cases} \tag{15}$$

The contact forces are associated with contact deformations. The Hertzian contact forces $Q_{in,j}$ and $Q_{out,j}$ between the jth ball and the inner and outer raceways are calculated by

$$Q_{in,j} = k_i \delta_{in,j}^{3/2} \tag{16}$$

$$Q_{out,j} = k_o \delta_{out,j}^{3/2} \tag{17}$$

where k_i and k_o are contact stiffness coefficients between balls and raceways, which depend on the curvatures of the ball and raceways. Detailed descriptions about the calculation of the contact stiffness coefficients can be referred to ref. [33].

3.2. Governing Equations of Motion

Once the contact forces and friction forces between balls and raceways were obtained, the dynamic differential equations of bearing components can be established. For the inner raceway, the sum of contact forces in the x and y directions are given by

$$N_{in,x} = \sum_{j=1}^{Z} Q_{in,j} \cos\theta_j \tag{18}$$

$$N_{in,y} = \sum_{j=1}^{Z} Q_{in,j} \sin\theta_j \tag{19}$$

The sum of friction forces in the x and y directions are written as

$$F_{in,x} = \sum_{j=1}^{Z} F_{in,j} \sin\theta_j \tag{20}$$

$$F_{in,y} = \sum_{j=1}^{Z} F_{in,j} \cos\theta_j \tag{21}$$

Therefore, the translational motions of the inner raceways in the x and y directions are defined by Newton's law

$$m_i\ddot{x}_s + c\dot{x}_s + N_{in,x} - F_{in,x} = W \tag{22}$$

$$m_i\ddot{y}_s + c\dot{y}_s + N_{in,y} - F_{in,y} = 0 \tag{23}$$

where m_i is the mass of the inner raceway (including the mass of shaft); c denotes the supporting damping coefficient; W refers to the radial load of bearing; Z means the number of balls.

For the jth ball, its dynamic motion in the radial direction is given as

$$m_r\ddot{d}_{br,j} + c\dot{d}_{br,j} + \left(Q_{out,j} - Q_{in,j}\right) = 0 \; j = 1, 2, 3, \ldots, Z \tag{24}$$

where m_r is the mass of the ball.

The rotational motion of the ball is described as

$$J_r\ddot{\theta}_{r,j} - \frac{1}{2}\left(F_{in,j} + F_{out,j}\right)D = 0 \; j = 1, 2, 3, \ldots, Z \tag{25}$$

where J_r is the moment of inertia of the ball.

4. Simulation Results and Discussion

The dynamic model described above includes $(2N_b + 2)$ differential equations for the bearing motion. The fourth-order Runge–Kutta algorithm with a constant time step ($\Delta t = 1 \times 10^{-5}$ s) was used to solve these equations. The solution process is shown in Figure 6. The bearing under investigation was a deep groove ball bearing (SKF 6304), and the parameters are given in Table 1. The initial displacements and velocities of the inner raceway were set to zero. Ball rotational speed obtained by simple kinematics was taken as its initial value.

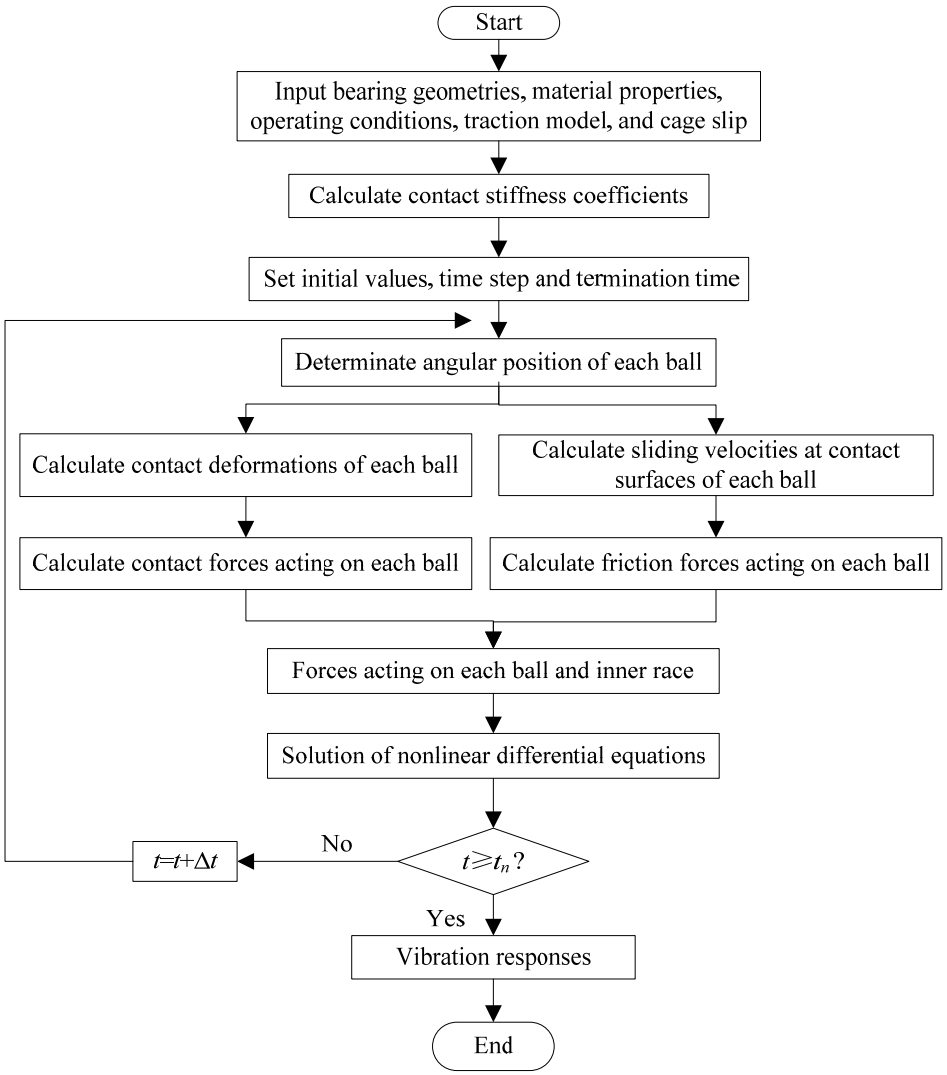

Figure 6. Flowchart of the solution process.

Table 1. Values of some parameters for the deep groove ball bearing.

Parameter	Value
Outer raceway diameter (d_o)	45.538 mm
Inner raceway diameter (d_i)	26.475 mm
Pitch diameter (d_m)	36 mm
Ball diameter (D)	9.525 mm
Number of balls (Z)	7
Radial clearance (P_d)	15 μm
Contact angle (α)	0°
Modulus of elasticity of bearing steel (E)	2.07×10^{11} Pa
Poisson's ratio of bearing steel (ν)	0.3
Mass of the inner raceway (m_i)	0.4 kg
Moment of inertia of ball (J_r)	3.18×10^{-8} kg·m^2
Damping coefficient (c)	350 Ns/m

4.1. Model Validation

In this section, the feasibility of the proposed dynamic model is verified by comparing simulated responses yielded by the proposed model with those obtained by Sunnersjo's model [4]. The dynamic model developed by Sunnersjo is a representative model to study bearing vibration. It considers the contact forces between balls and raceways based on pure

rolling assumption. In order to make the models comparable, a case without cage slip was chosen for comparison.

Figure 7a illustrates the acceleration of the inner raceway in the x-direction obtained by Sunnersjo's model at 2000 rpm rotating speed and 2000 N radial load. The simulated acceleration yield by the proposed model is shown in Figure 7b. It is found that the simulated response from the proposed model is consistent with those from Sunnersjo's model in terms of the time waveform shape and the amplitudes. Table 2 compares the statistical indicators including peak-to-peak value (PTP), root mean square (RMS), and kurtosis value of the response from these two models. The error between the two models is small, which verifies the proposed model.

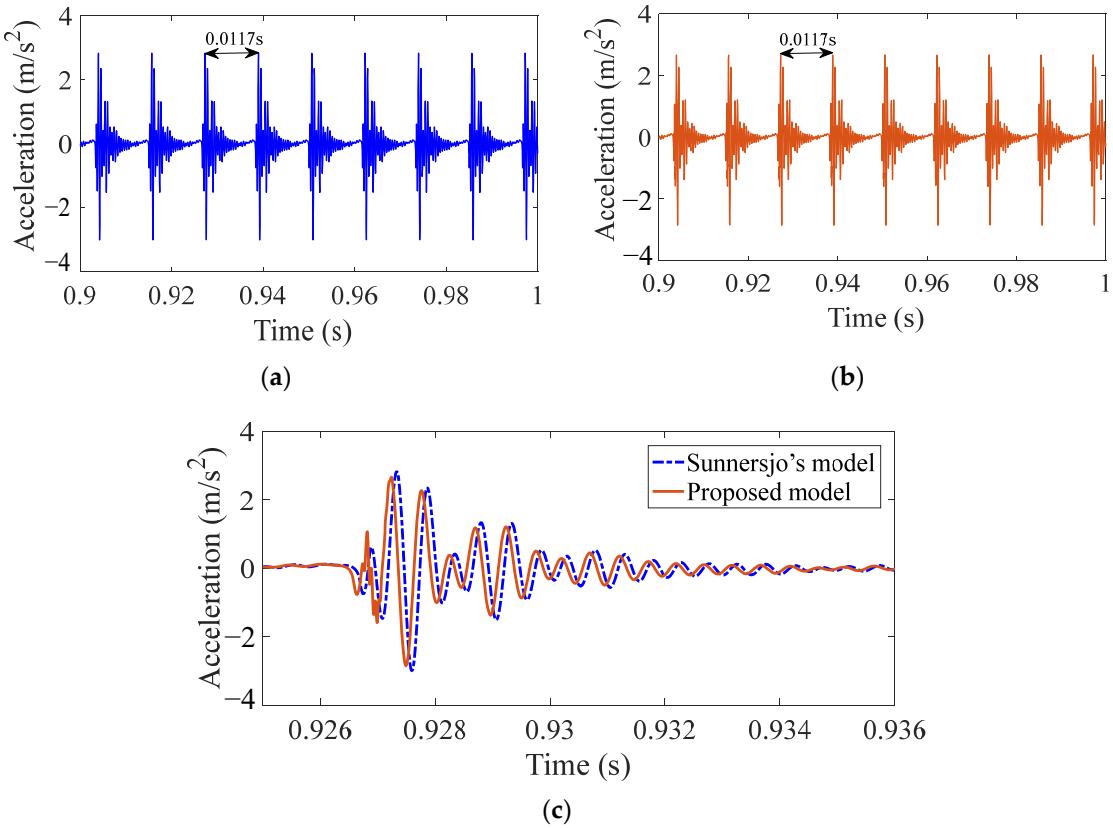

Figure 7. Acceleration of the inner raceway in the x-direction: (**a**) simulated vibration response by the Sunnersjo's model; (**b**) simulated vibration response by the proposed model; (**c**) comparison of the two models in one period.

Table 2. Comparison in terms of statistical indicators of acceleration response.

	X-Direction		
	PTP (m/s^2)	**RMS (m/s^2)**	**Kurtosis**
The proposed model	5.53	0.61	10.05
The Sunnersjo's model	5.84	0.65	9.79
Relative error (%)	5.31	6.15	2.66

Moreover, it is shown in Figure 7c that there are some discrepancies between the acceleration response obtained by the two models. The amplitude of the acceleration yielded by the proposed model is smaller than that of Sunnersjo's model. This may be caused by the friction considered in the model. According to Equations (9) and (10), relative slip between two contact surfaces generates friction force. Even under the situation of zero cage slip, there is still a slight sliding velocity between the rolling element and the

raceways. This friction makes the waveform shift to the right, compared with the waveform of Sunnersjo's model.

4.2. Friction Force Acting on the Ball Due to Cage Slip

The effect of cage slip on the acceleration of the inner raceway is dominated by the friction forces between the inner raceway and balls. The friction force is mainly dependent on the contact force, friction coefficient, and sliding velocity at the contact surface. Figure 8 shows the friction force applied to the first ball changing with its angular position. It can be observed that the friction force applied to the ball mainly appears in the loaded zone, and the waveform is similar to that of the load distribution of bearing. The maximum values of the friction force under different friction coefficients and cage slips are shown in Figure 9. As shown in Figure 9, when the friction coefficient is fixed, the maximum value of the friction force increases with the cage slip. The reason for this phenomenon is that the sliding velocity increases with the cage slip, and the friction coefficient also increases, as shown in Figure 4. Moreover, it can also be seen that when the cage slip is fixed, the maximum value of the friction force increases with the friction coefficient.

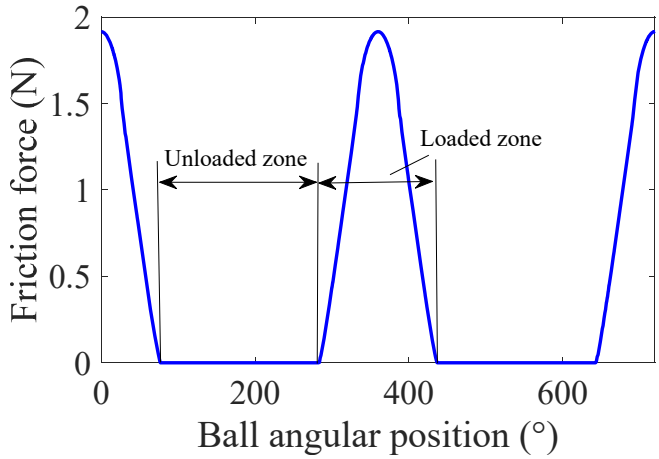

Figure 8. Friction force acting on the first ball versus angular position (ω_s = 2000 rpm, W = 2000 N, s_c = 2%, μ_m = 0.05).

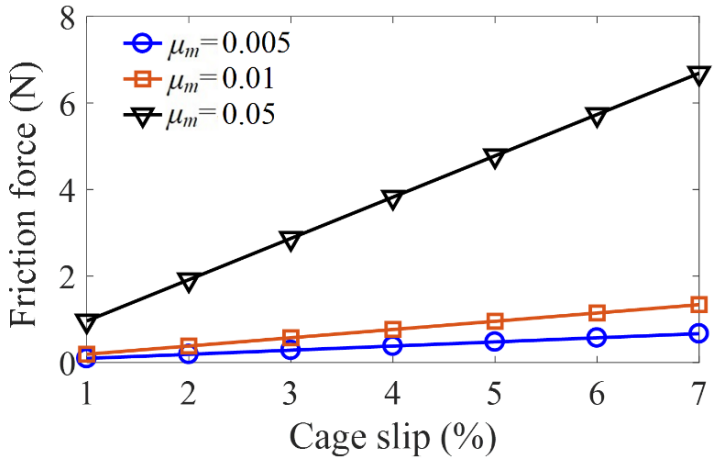

Figure 9. Effects of cage slip under different friction coefficients (ω_s = 2000 rpm, W = 2000 N).

Figure 10 shows the maximum values of the friction forces under different rotational speeds of inner raceway and radial loads. It is found that the maximum friction force increases with the radial load. This is because the contact force applied to the ball increases with the radial load. In addition, the maximum friction force increases with the inner

raceway speed. This can be attributed to the large sliding velocity when the raceway speed is high, as shown in equation (Equation (7)).

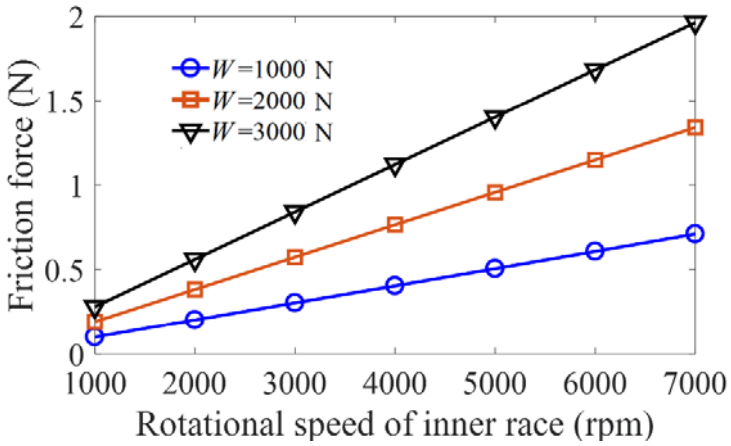

Figure 10. Effects of the rotational speed of inner raceway under different radial loads (s_c = 2%, μ_m = 0.01).

4.3. Dynamic Response Analysis

With the proposed model, the bearing vibration response was simulated and analyzed. The acceleration responses and their spectrums under different cage slips are illustrated in Figure 11. The most obvious change caused by the cage slip is the time interval between two adjacent cycles or the ball passing the outer raceway frequency (f_{bpo}). The ball passing the outer raceway frequency under the situation of no cage slip (85.5 Hz) is equal to the value determined by the calculation method in ref. [33]. The ball passing of the outer raceway frequency decreases with the cage slip. The correlation between the ball passing the outer raceway frequency and cage slip meets the following rule:

$$f_{bpo} = \frac{1}{2}(1 - s_c/100\%)(1 - \frac{D}{d_m}\cos\alpha)\omega_s Z \quad (26)$$

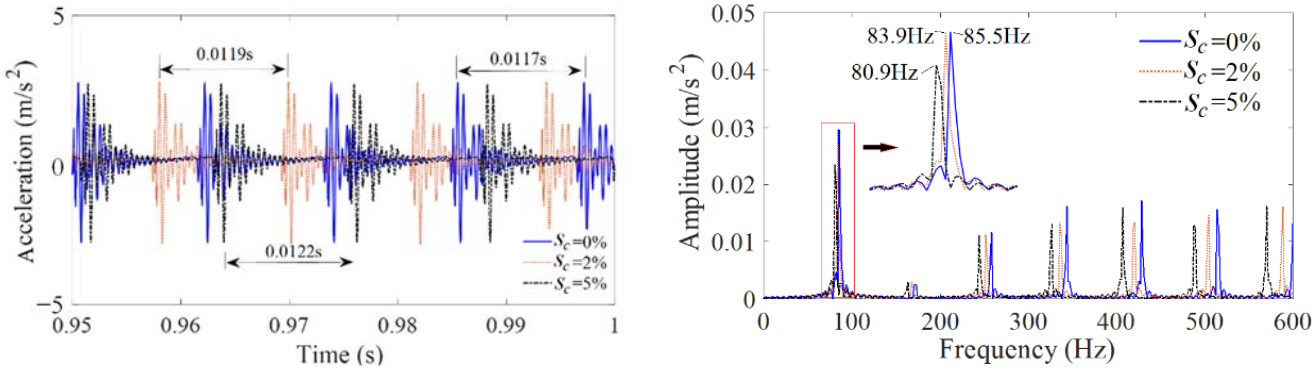

(**a**) (**b**)

Figure 11. Dynamic response of (**a**) time-domain waveforms and (**b**) their spectrums under different cage slip S_c (μ_m = 0.01, W = 2000 N, ω_s = 2000 rpm).

The effects of the rotational speed, the radial load, and the friction coefficient and cage slip on the bearing vibration response are investigated in this section. Three commonly used statistical indicators such as root mean square (RMS), peak-to-peak value (PTP), and kurtosis values were adopted to study the effects of cage slips on the bearing vibration response.

Figure 12 shows the statistical indicators of the acceleration response in the x-direction of the inner raceway under different cage slips and friction coefficients when the load W and rotating speed ω_s are 2000 N and 2000 rpm, respectively. It can be found that the RMS and PTP values of acceleration both decrease with the cage slip. This is probably because the friction forces applied to the inner raceway caused by the cage slip are in the opposite direction of the motion of the inner raceway. The friction forces could offset a portion of the contact forces and weaken the vibration energy. The vibration energy of the inner raceway decreases with the cage slip because of the friction forces acting on the inner raceway increase with the cage slip. This indicates that a small amount of cage slip could be helpful for the bearing vibration response. Moreover, when the cage slip is fixed, the RMS and PTP values of acceleration both increase with the friction coefficient when the friction is large enough, which means that the vibration energy increases with the friction coefficient. In addition, the kurtosis value increases with the cage slip and friction coefficient. The reason is that the impact components of acceleration response are induced by the friction forces.

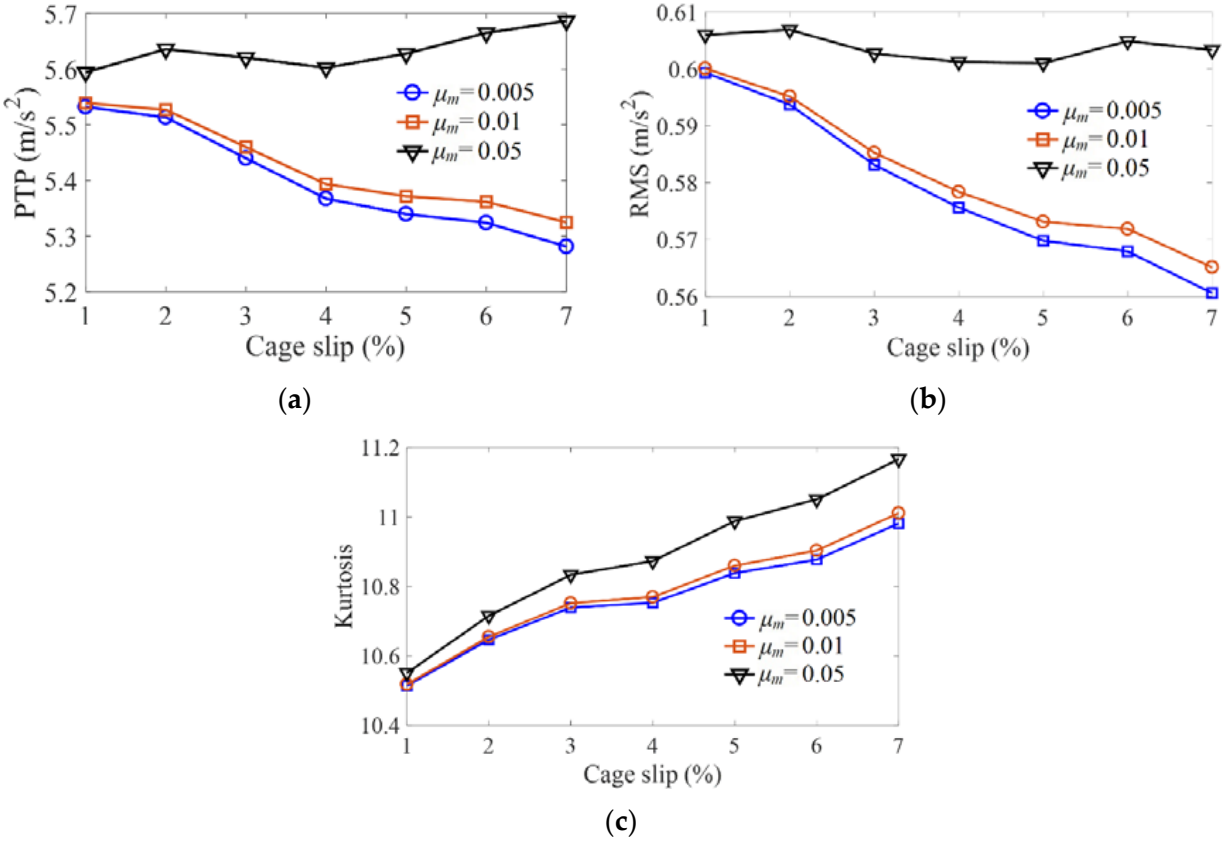

Figure 12. Effect of cage sip on statistical indicators of the acceleration of the inner raceway under different friction coefficients (W = 2000 N, ω_s = 2000 rpm): (**a**) PTP value; (**b**) RMS value; (**c**) kurtosis value.

The statistical indicators of the acceleration in the x-direction of the inner raceway under different rotational speeds and radial loads are illustrated in Figure 13, when the cage slip s_c and the friction coefficient μ_m are 2% and 0.01, respectively. It can be found that the RMS and PTP values of acceleration response both increase with rotational speeds. This can be also attributed to the friction forces, which increase with the rotational speeds. This leads one to infer that the vibration energy of the inner raceway increases with the inner raceway speed. Moreover, the RMS and PTP values of acceleration response increase with the growth of radial load at higher speeds, while they do not change significantly at lower speeds. In addition, the kurtosis value decreases when the inner raceway speed increases, and the change in the kurtosis value that occurs with the radial load is not obvious.

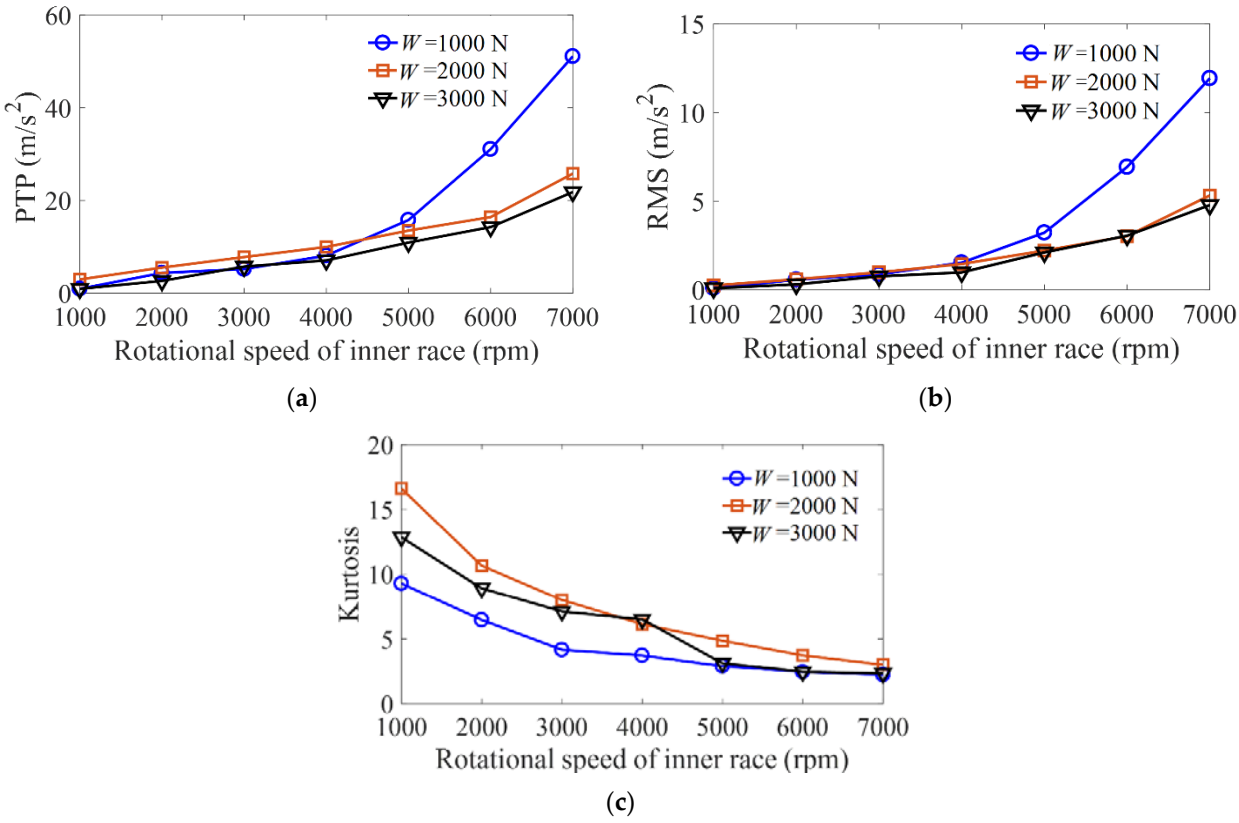

Figure 13. Effect of rotational speed on statistical indicators of the acceleration of the inner raceway under different radial loads W (s_c = 2%, μ_m = 0.01): (**a**) PTP value; (**b**) RMS value; (**c**) kurtosis value.

5. Conclusions

Aiming to settle the modeling problem of rolling-element bearing with cage slip, we established a nonlinear dynamic model with multiple degrees of freedom of rolling-element bearing, along with nonlinear contact, damping, and friction. The established model was verified by comparison with Sunnersjo's model under the situation of no cage slip. The friction force due to cage slip and the effect of cage slip on bearing vibration response were studied. The main conclusions of this research are drawn as follows:

(1) The friction force applied to the ball mainly appeared in the loaded zone. The peak value of the friction force increased with the cage slip, radial load, friction coefficient, and rotational speed;

(2) The RMS and PTP values of acceleration both decreased with the cage slip and increased with the friction coefficient. A minor cage slip was beneficial to the bearing vibration response. The kurtosis value increased with the cage slip and friction coefficient;

(3) When considering the cage slip, the RMS and PTP values of acceleration increased with the inner raceway speed and increased with the radial load only at high speeds. The kurtosis value decreased with the inner raceway speed. The variation trend of the kurtosis value with the radial load was not obvious.

Author Contributions: Conceptualization, Y.L. and W.T.; Data curation, Y.L. and W.T.; Funding acquisition, W.T. and W.Y.; Investigation, C.F. and L.Z.; Project administration, W.Y.; Supervision, W.T. and W.Y.; Writing—review & editing, Y.L., Y.Z. and W.Y. All authors have read and agreed to the published version of the manuscript.

Funding: This research was funded by the National Natural Science Foundation of China, grant number (51965018, 51905053, 52105086), and the Education Department Science and Technology Project of Jiangxi Province, grant number (GJJ200613).

Institutional Review Board Statement: Not applicable.

Informed Consent Statement: Not applicable.

Data Availability Statement: The data used to support the findings of this study are simulated by the proposed dynamic model. The values of model parameters are provided in the article so that readers can generate the simulation data by themselves. However, they are also available from the authors (wennian@cqu.edu.cn and twb-2001@163.com) upon request.

Acknowledgments: All of the authors would like to express their sincere gratitude to the funders of this research.

Conflicts of Interest: All of the authors declared that there are no potential conflict of interest concerning the authorship and publication of this study.

References

1. Ding, X.; Lin, L.; He, D.; Wang, L.; Huang, W.; Shao, Y. A Weight Multinet Architecture for Bearing Fault Classification under Complex Speed Conditions. *IEEE Trans. Instrum. Meas.* **2020**, *70*, 1–11. [CrossRef]
2. Tian, J.; Ai, Y.; Fei, C.; Zhao, M.; Zhang, F.; Wang, Z. Fault Diagnosis of Intershaft Bearings Using Fusion Information Exergy Distance Method. *Shock Vib.* **2018**, *2018*, 7546128. [CrossRef]
3. Tian, J.; Liu, L.; Zhang, F.; Ai, Y.; Wang, R.; Fei, C. Multi-Domain Entropy-Random Forest Method for the Fusion Diagnosis of Inter-Shaft Bearing Faults with Acoustic Emission Signals. *Entropy* **2019**, *22*, 57. [CrossRef] [PubMed]
4. Sunnersjö, C. Varying compliance vibrations of rolling bearings. *J. Sound Vib.* **1978**, *58*, 363–373. [CrossRef]
5. Zhang, Z.; Chen, Y.; Cao, Q. Bifurcations and hysteresis of varying compliance vibrations in the primary parametric resonance for a ball bearing. *J. Sound Vib.* **2015**, *350*, 171–184. [CrossRef]
6. Yang, R.; Hou, L.; Jin, Y.; Chen, Y.; Zhang, Z. The Varying Compliance Resonance in a Ball Bearing Rotor System Affected by Different Ball Numbers and Rotor Eccentricities. *J. Tribol.* **2018**, *140*, 051101. [CrossRef]
7. Jin, Y.; Yang, R.; Hou, L.; Chen, Y.; Zhang, Z. Experiments and Numerical Results for Varying Compliance Contact Resonance in a Rigid Rotor–Ball Bearing System. *J. Tribol.* **2017**, *139*, 041103. [CrossRef]
8. Tomović, R.; Miltenovic, V.; Banic, M.; Miltenović, A. Vibration response of rigid rotor in unloaded rolling element bearing. *Int. J. Mech. Sci.* **2010**, *52*, 1176–1185. [CrossRef]
9. Xi, S.; Cao, H.; Chen, X. Dynamic modeling of spindle bearing system and vibration response investigation. *Mech. Syst. Signal Process.* **2019**, *114*, 486–511. [CrossRef]
10. Tu, W.; Yang, J.; Yu, W.; Luo, Y. Contact characteristic and vibration mechanism of rolling element bearing in the process of fault evolution. *Proc. Inst. Mech. Eng. Part K J. Multi Body Dyn.* **2021**, *235*, 19–36. [CrossRef]
11. Kankar, P.K.; Sharma, S.C.; Harsha, S.P. Nonlinear vibration signature analysis of a high speed rotor bearing system due to raceway imperfection. *J. Comput. Nonlinear Dyn.* **2012**, *7*, 011014. [CrossRef]
12. Shah, D.S.; Patel, V.N. Theoretical and experimental vibration studies of lubricated deep groove ball bearings having surface waviness on its raceways. *Measurement* **2018**, *129*, 405–423. [CrossRef]
13. Liu, J.; Li, X.; Yu, W. Vibration analysis of the axle bearings considering the combined errors for a high-speed train. *Proc. Inst. Mech. Eng. Part K J. Multi Body Dyn.* **2020**, *234*, 481–497. [CrossRef]
14. Jing, L.; Ruikun, P.; Yajun, X.; Shizhao, D.; Qubo, H. Vibration analysis of a single row angular contact ball bearing with the coupling errors including the surface roundness and waviness. *Sci. China Technol. Sci.* **2020**, *63*, 943–952.
15. Yu, X.; Sun, Y.; Zhao, D.; Wu, S. A revised contact stiffness model of rough curved surfaces based on the length scale. *Tribol. Int.* **2021**, *164*, 107206. [CrossRef]
16. Singh, S.; Köpke, U.G.; Howard, C.Q.; Petersen, D. Analyses of contact forces and vibration response for a defective rolling element bearing using an explicit dynamics finite element model. *J. Sound Vib.* **2014**, *333*, 5356–5377. [CrossRef]
17. Li, X.; Yu, K.; Ma, H.; Cao, L.; Luo, Z.; Li, H.; Che, L. Analysis of varying contact angles and load distributions in defective angular contact ball bearing. *Eng. Fail. Anal.* **2018**, *91*, 449–464. [CrossRef]
18. Shah, D.S.; Patel, V.N. A dynamic model for vibration studies of dry and lubricated deep groove ball bearings considering local defects on raceways. *Measurement* **2019**, *137*, 535–555. [CrossRef]
19. Liu, J.; Xu, Z.; Xu, Y.; Liang, X.; Pang, R. An analytical method for dynamic analysis of a ball bearing with offset and bias local defects in the outer raceway. *J. Sound Vib.* **2019**, *461*, 114919. [CrossRef]
20. Liu, J.; Xu, Z.; Zhou, L.; Yu, W.; Shao, Y. A statistical feature investigation of the spalling propagation assessment for a ball bearing. *Mech. Mach. Theory* **2019**, *131*, 336–350. [CrossRef]
21. Qin, Y.; Li, C.; Cao, F.; Chen, H. A fault dynamic model of high-speed angular contact ball bearings. *Mech. Mach. Theory* **2019**, *143*, 103627. [CrossRef]
22. Tu, W.; Luo, Y.; Yu, W.; Yu, Y. Investigation of the dynamic local skidding behaviour of rollers in cylindrical roller bearings. *Proc. Inst. Mech. Eng. Part K J. Multi Body Dyn.* **2019**, *233*, 899–909. [CrossRef]
23. Sawalhi, N.; Randall, R. Simulating gear and bearing interactions in the presence of faults: Part I. The combined gear bearing dynamic model and the simulation of localised bearing faults. *Mech. Syst. Signal Process.* **2008**, *22*, 1924–1951. [CrossRef]

24. Niu, L.; Cao, H.; He, Z.; Li, Y. A systematic study of ball passing frequencies based on dynamic modeling of rolling ball bearings with localized surface defects. *J. Sound Vib.* **2015**, *357*, 207–232. [CrossRef]
25. Tu, W.; Luo, Y.; Yu, W. Dynamic Interactions Between the Rolling Element and the Cage in Rolling Bearing Under Rotational Speed Fluctuation Conditions. *J. Tribol.* **2019**, *141*, 091101. [CrossRef]
26. Tu, W.; Yu, W.; Shao, Y.; Yu, Y. A nonlinear dynamic vibration model of cylindrical roller bearing considering skidding. *Nonlinear Dyn.* **2021**, *103*, 2299–2313. [CrossRef]
27. Liu, Y.; Chen, Z.; Tang, L.; Zhai, W. Skidding dynamic performance of rolling bearing with cage flexibility under accelerating conditions. *Mech. Syst. Signal Process.* **2021**, *150*, 107257. [CrossRef]
28. Wang, Y.; Wang, W.; Zhang, S.; Zhao, Z. Investigation of skidding in angular contact ball bearings under high speed. *Tribol. Int.* **2015**, *92*, 404–417. [CrossRef]
29. Han, Q.; Chu, F. Nonlinear dynamic model for skidding behavior of angular contact ball bearings. *J. Sound Vib.* **2015**, *354*, 219–235. [CrossRef]
30. Han, Q.; Li, X.; Chu, F. Skidding behavior of cylindrical roller bearings under time-variable load conditions. *Int. J. Mech. Sci.* **2018**, *135*, 203–214. [CrossRef]
31. Selvaraj, A.; Marappan, R. Experimental analysis of factors influencing the cage slip in cylindrical roller bearing. *Int. J. Adv. Manuf. Technol.* **2010**, *53*, 635–644. [CrossRef]
32. Zhan, L.; Ma, F.; Li, Z.; Li, H.; Li, C. Study on the cage slip of rolling bearing using a non-contact method. *Struct. Health Monit.* **2020**, *19*, 2107–2121. [CrossRef]
33. Harris, T.A.; Kotzalas, M.N. *Rolling Bearing Analysis: Essential Concepts of Bearing Technology*; Taylor & Francis: Boca Raton, FL, USA, 2007.
34. Bujoreanu, C.; Cretu, S.; Nelias, D. Scuffing behaviour in angular contact ball-bearings. *Ann. Univ. Dunărea Jos Galaţi Fascicle Viii Tribol.* **2003**, *2*, 33–39.
35. Gupta, P.K. *Advanced Dynamics of Rolling Elements*; Springer Science & Business Media: Berlin/Heidelberg, Germany, 1984. [CrossRef]
36. Bălan, M.R.D.; Stamate, C.; Houpert, L.; Olaru, D.N. The influence of the lubricant viscosity on the rolling friction torque. *Tribol. Int.* **2014**, *72*, 1–12. [CrossRef]
37. Olaru, D.; Puiu, G.C.; Balan, L.C.; Puiu, V. A New Model to Estimate Friction Torque in a Ball Screw System. In *Product Engineering*; Springer: Dordrecht, The Netherlands, 2006; pp. 333–346. [CrossRef]
38. Ghaisas, N.; Wassgren, C.R.; Sadeghi, F. Cage Instabilities in Cylindrical Roller Bearings. *J. Tribol.* **2004**, *126*, 681–689. [CrossRef]
39. Takabi, J.; Khonsari, M.M. On the Influence of Traction Coefficient on the Cage Angular Velocity in Roller Bearings. *Tribol. Trans.* **2014**, *57*, 793–805. [CrossRef]